The Astrophysical Journal, 697:106–114, 2009 May 20 doi:10.1088/0004-637X/697/1/106

PROPAGATION AND SOURCE ENERGY SPECTRA OF COSMIC RAY NUCLEI AT HIGH ENERGIES

M. Ave, P. J. Boyle[1], C. Höppner[2], J. Marshall, and D. Müller
Enrico Fermi Institute, The University of Chicago, 933 E 56th Street, Chicago, IL 60637, USA; boyle@uchicago.edu
Received 2008 October 16; accepted 2009 March 6; published 2009 April 30

ABSTRACT

A recent measurement of the TRACER instrument on long-duration balloon has determined the individual energy spectra of the major primary cosmic ray nuclei from oxygen ($Z = 8$) to iron ($Z = 26$). The measurements cover a large range of energies and extend to energies beyond 10^{14} eV. We investigate if the data set can be described by a simple but plausible model for acceleration and propagation of cosmic rays. The model assumes a power-law energy spectrum at the source with a common spectral index α for all nuclear species, and an energy-dependent propagation path length ($\Lambda \propto E^{-0.6}$) combined with an energy-independent residual path length Λ_0. We find that the data can be fitted with a fairly soft source spectrum ($\alpha = 2.3$–2.4), and with a residual path length Λ_0 as high as 0.3 g cm^{-2}. We discuss this model in the context of other pertinent information, and we determine the relative abundances of the elements at the cosmic ray source.

Key words: acceleration of particles – cosmic rays – ISM: abundances

1. INTRODUCTION

Measurements of the composition and energy spectra of cosmic rays, whether with instruments above the atmosphere or with air-shower installations on the ground, characterize the cosmic ray population after the particles have traveled from their acceleration sites (the "sources") through distant space and through the solar system. Both the composition of the particles and the shapes of their energy spectra undergo changes due to a variety of processes during propagation. It has long been a challenge to understand these changes and thereby to develop a self-consistent model that connects detailed observational data with the characteristics of the cosmic ray sources.

The most detailed observations of cosmic rays have been made at relatively low energies, from the subrelativistic region (less than 100 MeV amu^{-1}) to a few GeV amu^{-1}. These measurements have even revealed the isotopic composition of cosmic ray nuclei (e.g., Wiedenbeck et al. 1998; Yanasak et al. 2001), and hence allow a much more specific analysis than possible at higher energies. However, the propagation effects in this energy region are quite complex: the interaction cross sections are energy dependent, the particles are subject to ionization loss rates which increase with decreasing energy; and the particle intensities and energies are subject to solar modulation. Not all parameters that characterize these processes are well known.

At relativistic energies (above a few GeV amu^{-1}), the propagation parameters are much easier to characterize, but due to the steeply falling energy spectra, cosmic ray measurements require very large detector systems and are often statistics limited. While isotopic resolution has not been achieved in this region, recent data on the elemental composition of cosmic ray nuclei reach up to energies around 10 TeV amu^{-1}. Thus, data are now available for three decades in energy above the region of solar modulation. With the present study, we wish to investigate whether the measurements can be interpreted in the context of a simple and physically plausible model of cosmic ray acceleration and propagation. One would like to extend the analysis into the region of air-shower measurements, i.e., the five decades of energy above the cosmic ray "knee." However, the interpretation of these data is difficult because of uncertainties in the hadronic interaction process and in the identification of the primary particles.

2. THE MEASUREMENTS

Measurements of the individual energy spectra of cosmic ray nuclei heavier than protons and helium at high energies have been performed with two missions in space: *HEAO-3* which provided data with high statistical accuracy up to about 35 GeV amu^{-1} (Engelmann et al. 1990), and CRN on *Spacelab-2* which performed the first measurements into the TeV amu^{-1} region (Müller et al. 1991). In addition, several balloon-borne instruments have performed composition measurements in this region: JACEE (Asakimori et al. 1998), RUNJOB (Derbina et al. 2005), ATIC (Panov et al. 2006), CREAM (Seo et al. 2006), and TRACER (Ave et al. 2008).

For this study, we use the TRACER data set as it covers the major primary heavy nuclei with individual charge resolution and extends up to very high energies. The data set includes the energy spectra of the elements O, Ne, Mg, Si, S, Ar, Ca, and Fe over the energy range from a few GeV amu^{-1} to more than 10^4 GeV amu^{-1}. The differential energy spectra are shown in Figure 1. The figure also includes the measurements made in space with the *HEAO-3* and *Spacelab-2* instruments. There seems to be general agreement between the results of these three measurements in the energy region where overlap exists. As pointed out earlier (Ave et al. 2008), the preliminary results of the other balloon instruments agree with the trend of the TRACER data.

We had reported previously (Ave et al. 2008) that the combination of the energy spectra from the TRACER and CRN measurements, above 20 GeV amu^{-1}, can be reasonably well fitted to a single power law $\propto E^{-\Gamma}$, with common exponent $\Gamma = 2.65 \pm 0.05$. Figure 2 shows this analysis for the TRACER data alone leading to an average exponent of 2.67 ± 0.08. While this behavior may strongly suggest a common origin of all cosmic ray species, one must expect that it can only be true in approximation. Closer examination leads one to expect that the competing action of physical escape from the Galaxy, which depends on energy, and of loss by spallation in the interstellar

[1] Author to whom any correspondence should be addressed.
[2] Current address: Technische Universität München, München, Germany.

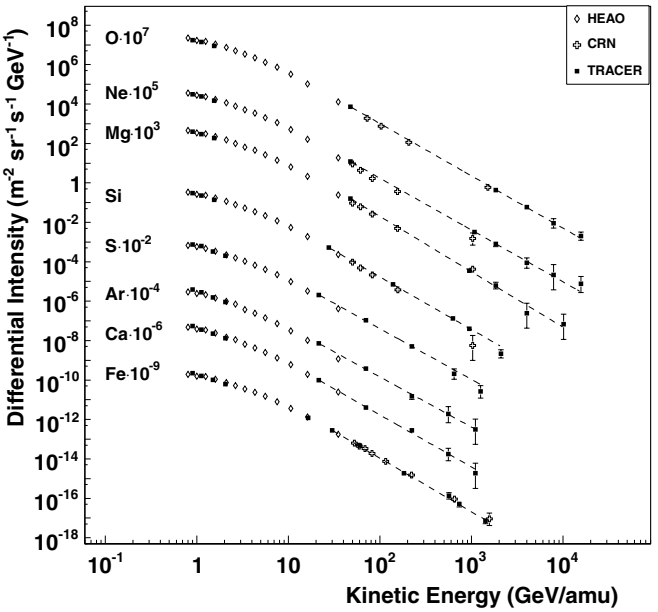

Figure 1. Differential energy spectra for the cosmic ray nuclei O, Ne, Mg, Si, S, Ar, Ca, and Fe. Results from TRACER are indicated by the solid squares, *HEAO-3* by open diamonds, and CRN by open crosses. The dashed line represents an independent power-law fit to each spectrum above 20 GeV amu^{-1}.

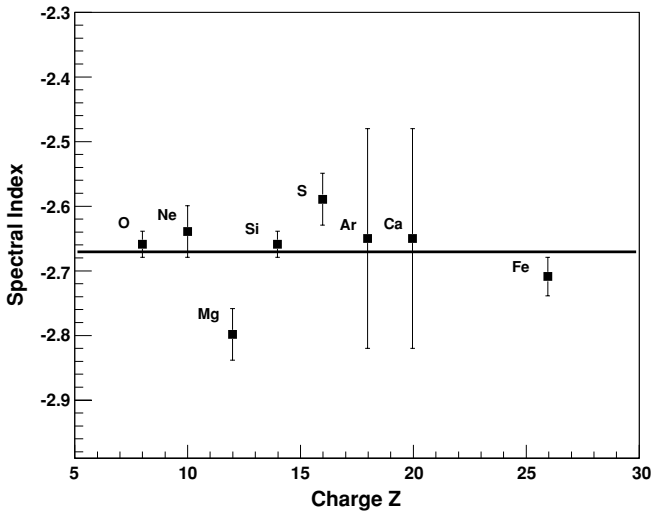

Figure 2. Spectral indices of a best power-law fit to the TRACER data above 20 GeV amu^{-1}. The line indicates an average spectral fit of $E^{-2.67}$.

medium (ISM), which depends on the nuclear charge Z (or more correctly, on atomic number A), leads to subtle changes in the spectral shape for individual nuclei that would be difficult to describe by a single power-law spectrum. Details of these effects will be discussed in the following study.

3. PROPAGATION MODEL

3.1. Leaky Box Approximation

It is generally assumed that the cosmic rays are continuously produced in the galaxy, and that their population in the ISM results from dynamic equilibrium between the rates with which they are released from the sources or generated as secondaries in the ISM, and with which they are lost from the galactic disk. Loss processes include diffusion or convection, energy losses or gains, nuclear interactions with particles of the ISM, and possibly radioactive decay.

The situation is commonly summarized in a continuity equation for the differential density $N_i(E)$ of each component, where E denotes the kinetic energy per amu (e.g., Ginzburg & Syrovatskii 1964):

$$\begin{aligned} Q_i(E) + \sum_{k>i} \frac{\beta c \rho}{m} \int_{E'>E} \frac{d\sigma_{k\to i}(E, E')}{dE'} N_k(E') dE' \\ = \; -\nabla(D_i(E)\nabla N_i(E)) \\ + \; \frac{\partial}{\partial E}(b_i(E) N_i(E)) \\ + \; \nabla \cdot \vec{u} N_i(E) + \frac{\beta c \rho}{\Lambda_i} N_i(E) + \frac{1}{\gamma T_i} N_i(E). \end{aligned}$$

The left-hand side of the equation includes $Q_i(E)$, the rate of production in the source, and a term for secondary production in the ISM, with ρ the mass density of the interstellar gas, $\beta = v/c$, m the average mass of an interstellar target atom in grams, and $d\sigma_{k\to i}(E, E')/dE'$ the differential cross section for spallation of component k at energy E' into component i at energy E. The right-hand side describes the loss processes in the same order as listed above, with $D_i(E)$ the diffusion coefficient, b_i the rate of energy loss, $\vec{u}$ the speed of convection, Λ_i the spallation mean free path Λ_i, Lorentz factor γ, and the radioactive decay time T_i.

The number of free or unknown parameters in this equation is large, and drastic simplifications are usually made to treat the cosmic ray problem. Perhaps most difficult is the treatment of the diffusion term which summarizes the interaction between the cosmic ray particle and the stochastic interstellar magnetic fields. The situation is simplified by introducing the average containment time $\tau(E)$ of particles in the galaxy or, equivalently, the propagation path length $\Lambda(E)$ is

$$\Lambda(E) = \beta c \rho \tau(E), \tag{1}$$

where $\beta \approx 1$ in the energy region of concern and Λ and τ are assumed to be averages of exponential distributions. In principle, the containment time can be measured directly through the observation of radioactive nuclei, and such measurements have been highly successful at low energies, yielding $\tau \approx 1.5 \times 10^7$ years below 1 GeV amu^{-1} (first reported by Garcia Muñoz et al. 1975; confirmed in more recent work, for instance, Yanasak et al. 2001). As discussed below, $\Lambda(E)$ has been observed to decrease with energy E, and according to Equation (1), $\tau(E)$ would follow this trend.

Similarly, one may introduce an average spallation path length $\Lambda_s(A)$ to describe the loss of nuclei due to spallation:

$$\Lambda_s(A) = m/\sigma(A), \tag{2}$$

where m is the average mass of an interstellar target nucleus, measured in grams, and $\sigma(A)$ is the spallation cross section, measured in square centimeters, of a cosmic ray nucleus with mass number A. It is usually assumed that spallation produced nuclei have the same energy per amu as their parent nuclei.

If convection effects are neglected (probably a valid approximation at high energies), as well as effects due to energy gain or loss (including re-acceleration in the ISM), and radioactive decay, the continuity equation becomes

$$N_i(E) = \frac{1}{\Lambda(E)^{-1} + \Lambda_s(A)^{-1}} \left(\frac{Q_i(E)}{\beta c \rho} + \sum_{k>i} \frac{N_k}{\Lambda_{k\to i}} \right). \tag{3}$$

Here, $\Lambda_{k\rightarrow i}$ quantifies the probability of a nucleus k to spallate into a product i in an interstellar interaction. Equation (3) appears to be much more manageable than Equation (1) and is often called the "leaky box" approximation. Its major shortcomings are twofold. (1) The diffusion boundaries, i.e., the shape and structure of the Galaxy and its halo, are ignored. (2) The cosmic ray source $Q(E)$ is assumed to be continuous, although at any given time, only a relatively small number (less than 100) of sources can be active if discrete supernova remnants (SNRs) are the accelerators of cosmic rays. However, as the galactic containment time of cosmic rays exceeds the active lifetime of an SNR by at least a factor of 10^3, the number of galactic sources contributing to the equilibrium cosmic ray population could be of order 10^5.

Nevertheless, in the following, Equation (3) is used as a base for describing the recent measurement of cosmic ray nuclei at high energies.

3.2. Diffusion and Spallation

At relativistic energies ($\geqslant$ few GeV amu^{-1}), the diffusion coefficient describing the propagation of cosmic rays through the galaxy increases with energy. The observational evidence for this fact, first reported in the early 1970s (Juliusson et al. 1972; Smith et al. 1973), comes from measurements of the relative abundances of spallation produced secondary cosmic ray nuclei; most detailed are measurements of the abundance of boron ($Z = 5$), relative to its parents carbon and oxygen ($Z = 6, 8$). Figure 3 shows measurements obtained in space with the *HEAO-3* (Engelmann et al. 1990) and CRN/*Spacelab-2* missions (Swordy et al. 1990), and also more recent measurements by the balloon-borne CREAM instrument (Ahn et al. 2008). These measurements can be parameterized (Swordy et al. 1990) with a propagation path length Λ that decreases with energy proportional to $R^{-0.6}$ (where R is the particle rigidity):

$$\Lambda(R) = 6.9\left(\frac{R}{20\ \mathrm{GV}}\right)^{-0.6}\ \mathrm{g\ cm^{-2}}, \quad (R > 20\ \mathrm{GV}). \qquad (4)$$

Note that the rigidity is defined as $R = pc/Ze$, with momentum p, and the charge of the nucleus Ze. For highly relativistic particles ($\gamma \gg 1$), the kinetic energy per amu is proportional to R; E per amu $= (Z/A)eR$. Few physical mechanisms have been proposed that could lead to this power-law dependence of the escape path length Λ on rigidity or energy (e.g., Ptuskin et al. 1997). Further, the currently available data become quite uncertain above about 100 GeV amu^{-1}. The energy dependence at lower energies, $\leqslant$10 GeV amu^{-1}, has been studied by Yanasak et al. (2001), and parameterized in the form

$$\Lambda(R) = \frac{26.7\beta}{(\beta R)^{0.58} + (0.714 \times \beta R)^{-1.4}}\ \mathrm{g\ cm^{-2}}, \qquad (5)$$

At high energies, Equations (4) and (5) yield essentially the same trend with energy (although the path length according to Equation (4) is larger than that calculated by Equation (5) by about 25%). It is unlikely, however, that the power-law behavior persists to the highest energies: the diminishing path length would be difficult to reconcile with the observed isotropy of the cosmic ray flux. Taking this into account, we introduce a residual path length Λ_0 that would be reached asymptotically at high energies:

$$\Lambda(R) = C\,R^{-0.6} + \Lambda_0. \qquad (6)$$

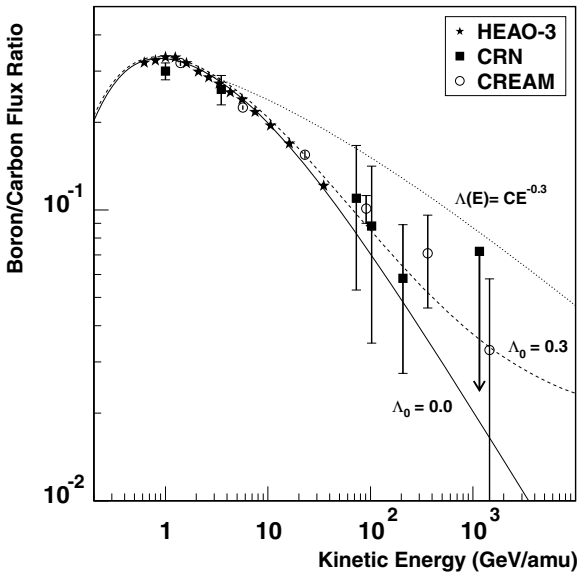

Figure 3. Boron to carbon flux ratio with data from *HEAO-3*, CRN, and CREAM. The solid line represents the parameterization from Equation (5). The addition of a residual path length of $\Lambda_0 = 0.3$ g cm^{-2} is indicated by the dashed line, and $\Lambda(E) \propto E^{-0.3}$ is shown as the dotted line.

This would reflect the fact that even at extremely high energies, the cosmic rays must traverse a minimum amount of galactic matter.

To obtain numerical values for the spallation path length $\Lambda_s(A)$ (Equation (2)), it is assumed that the interstellar gas consists of 90% hydrogen and 10% helium. For a given nucleus $\Lambda_s(A)$ can therefore be written as

$$\Lambda_s(A) = \frac{2.17 \times 10^{-24}}{0.9\sigma_{\mathrm{H}}(A) + 0.1\sigma_{\mathrm{He}}(A)}\ \mathrm{g\ cm^{-2}}, \qquad (7)$$

where the *total* cross sections for charge–changing interactions of this nucleus are $\sigma_{\mathrm{H}}(A)$ and $\sigma_{\mathrm{He}}(A)$ on hydrogen or helium targets, respectively. The cross sections have been determined empirically. In the following analysis, the measured and interpolated values from Webber et al. (1990) at an energy of 1.5 GeV amu^{-1} are used. Although there are very few cross section measurements available at higher energies, a slight increase in cross section with energy may be possible, but would not significantly affect our conclusions (Hörandel et al. 2006 quote $\sigma \propto E^{+\varepsilon}$ with ε of the order of 10^{-2}).

The partial path lengths $\Lambda_{k\rightarrow i}$ in Equation (3) are calculated using *partial* cross sections in Equation (2) that are derived from the semiempirical formula of Webber et al. (2003). This formula computes the cross section of an interaction on a hydrogen target, and allows for the extrapolation to 6 GeV amu^{-1}, above which the cross sections are taken as energy independent. The semiempirical formula agrees with most cross sections measured by Webber et al. (2003) within 5%; however, in some cases Villagrasa-Canton et al. (2007) have reported deviations greater than 20%. Furthermore, the semiempirical cross sections do not include the helium component of the ISM. Therefore, in the following analysis a conservative systematic uncertainty of 25% is assigned to the partial cross sections.

The two quantities $\Lambda(R)$ and $\Lambda_s(A)$ characterize the propagation of cosmic rays. The propagation path length decreases with energy but is assumed to have the same value for different nuclei of the same rigidity or energy per amu. The spallation

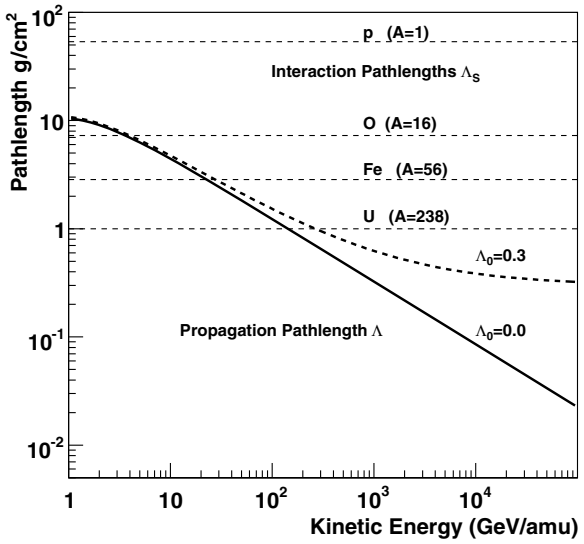

Figure 4. Comparison of the escape path length from Equation (5) (solid and dashed curves) and interaction path length (dashed lines). The interaction path lengths are given for several elements including, for illustration, protons and uranium.

path length, on the other hand, depends on the atomic number A (essentially $\Lambda_s \propto A^{-2/3}$) but its energy dependence is very weak for relativistic particles, and is ignored in this study.

In Figure 4, the values for $\Lambda(R)$ and $\Lambda_s(A)$ are summarized. As can be seen, the path lengths $\Lambda(R)$ and $\Lambda_s(A)$ are of comparable magnitude in the energy region 5–20 GeV amu^{-1} for the nuclei oxygen to iron. For comparison, the value of the interaction path length for protons is indicated, which is much larger than $\Lambda(R)$ for all energies, and for uranium, which becomes larger than $\Lambda(R)$ only above about 100 GeV amu^{-1}.

Equation (3), if valid, shows that the smaller of the two path lengths dominates the fate of cosmic rays during propagation: for protons, this is the escape path length $\Lambda(R)$ practically for all energies, while for the heavier nuclei, the escape path length dominates only at sufficiently high energies.

4. FIT OF DATA TO PROPAGATION MODEL

4.1. Choice of Input Parameters to the Model

We wish now to fit the cosmic ray energy spectra measured by TRACER with the simple model just described. A number of parameters must, however, be chosen before Equation (3) can be applied for a comparison with measured data. The following assumptions are made.

1. All primary cosmic ray nuclei are assumed to be accelerated by the same mechanism, such that the source rigidity spectrum, $Q_i(R) = n_i R^{-\alpha}$, has the same power-law index α for all elements. This is consistent with simple shock acceleration models if $\alpha \geqslant 2.0$. At relativistic energies the distinction between rigidity and energy can be ignored and the source energy spectrum is $\propto E^{-\alpha}$. The parameter α is left free to vary when the fitting procedure is applied to the measured data.
2. The quantities n_i reflect the abundances of the cosmic ray species at the sources. Numerical values for n_i will be determined in the fitting procedure to the data.
3. The propagation path length $\Lambda(R)$ is assumed to decrease with rigidity like $R^{-0.6}$ in accordance with Equations (4) and (5). Specifically, the formulation of Equation (5) is used in the fit procedure. In addition, an allowance is made for a residual energy-independent contribution by adding a value Λ_0 to Equation (5) (as in Equation (6)). Λ_0 is treated as a free parameter, and constraints on its numerical value will be derived from the measured data.

4.2. The Propagation Network

The goal of the computational procedure is to find a pair of values (α, Λ_0) that provides a best fit to the energy spectra of all nuclear species. The calculation begins with the heaviest element, iron, assuming that the nearly all arriving iron comes from the cosmic ray source (i.e., there is a small allowance for secondary iron from the spallation of nickel). For a given pair of constants α and Λ_0, Equation (3) is used to calculate the arriving iron energy spectrum $N_{\rm Fe}(E)$, and the source abundance $n_{\rm Fe}$ is varied until a best fit to the data is achieved. The measured iron spectrum from Ave et al. (2008) for energies above 10 GeV amu^{-1} is used in this procedure. A best fit is determined by maximizing the likelihood ratio $\lambda_{\rm Fe}(\alpha, \Lambda_0, n_{\rm Fe})$,[3] or equivalently by minimizing the parameter $\chi^2_{\rm Fe}(\alpha, \Lambda_0, n_{\rm Fe})$[4] (Baker & Cousins 1984). Using this "best-fit" iron spectrum $N_{\rm Fe}(E)$, the intensities of secondary nuclei are computed from the spallation of iron to all species with lower mass number than iron.

An identical calculation is then performed, for the same values of α and Λ_0, successively for all nuclei with lower charge. To include minor contributions of rare and odd-Z elements that are not measured by TRACER, calculations for these elements use the relative source abundances derived from the *HEAO-3* experiment. At the end of this process, *for a chosen* (α, Λ_0) *combination*, a set of eight values of χ^2_i is obtained for the fits to the eight measured elemental species, together with a set of eight source abundances n_i.

The procedure is then repeated for a variety of choices of source spectral indices α and residual path length Λ_0. Figure 5 shows an example of the results: shown here is a contour plot of χ^2_i values for the elements oxygen and iron over the α–Λ_0 plane. The minimum values of χ^2_i are indicated in the plot. However, the minima are not very well defined, rather good-fit results for (α, Λ_0) lie along a valley in the α–Λ_0 plane. The position of the valley is not identical for the two elements, but significant overlap exists. Before drawing any conclusion, the results shown in Figure 5 must be combined with those obtained for the other elemental species.

4.3. Combined Fit

The procedure just described yields contour maps in the α–Λ_0 plane similar to those shown in Figure 5 for all cosmic ray elements whose energy spectra are given in Figure 1. Note that only the data obtained with the TRACER instrument are used, and that the analysis is restricted to energies above 10 GeV amu^{-1} in order to avoid complications due to solar modulation.

We now investigate which values of (α, Λ_0), if any, would provide an acceptable fit to all data combined. To this end, we define a combined value $\chi^2 = \sum \chi^2_i$ for each combination of (α, Λ_0). A combined χ^2 map is then constructed and is shown in Figure 6 together with the 1σ and 3σ contours.[5] Once again, the best fit to the combined data is found to lie along a valley

[3] $\lambda_{\rm Fe}(\alpha, \Lambda_0, n_{\rm Fe}) = \prod(\frac{P(m_j, m_j')}{P(m_j, m_j)})$, where m_j is the measured data in bin j, m_j' is the simulated data in bin j, and P is the Poisson distribution.

[4] $\chi^2_{\rm Fe}(\alpha, \Lambda_0, n_{\rm Fe}) = -2 \ln \lambda_{\rm Fe}$.

[5] The 1σ and 3σ contours are defined as $\Delta\chi^2 = 2.3$ and 11.83, respectively.

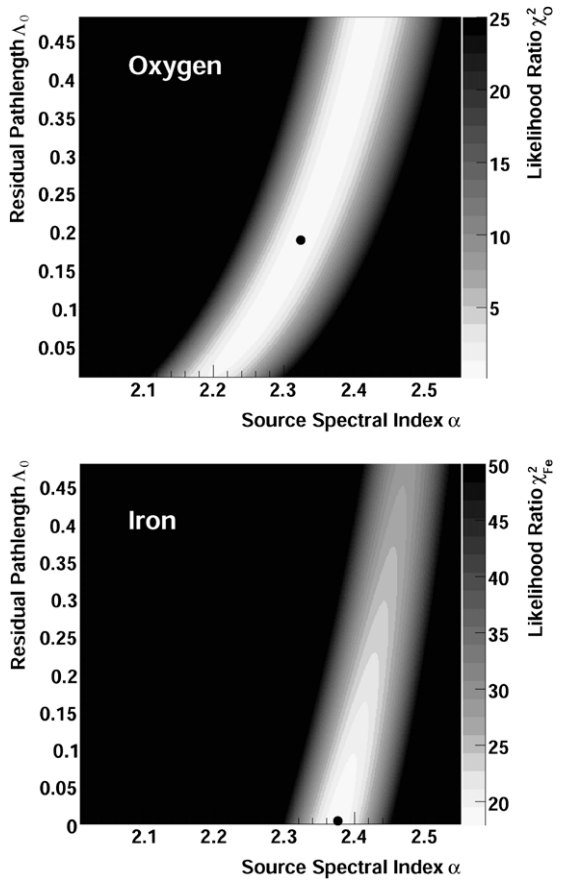

Figure 5. Contour maps of χ^2 values for oxygen (upper) and iron (lower). The minimum for each plot is represented by the black filled circle.

in the α–Λ_0 plane. This valley extends from spectra with (α, Λ_0) = (2.35, 0.1 g cm^{-2}) to perhaps (2.45, 0.6 g cm^{-2}) [3σ]. Baseline values of (α, Λ_0) = (2.4, 0.3 g cm^{-2}) are chosen for our description of the cosmic ray energy spectra. To further constrain the choice of (α, Λ_0) along the valley, additional information is required and will be discussed in Section 6.

To illustrate the quality of the fit, Figure 7 shows the individual energy spectra for all elements, multiplied with $E^{2.65}$, with the model fits indicated by the solid curves. It is interesting to note that the propagation model also computes the secondary contributions to each of the individual spectra. These are shown as dashed lines in Figure 7. As expected, the relative intensity of the secondaries decreases with increasing energy. It is generally in the order of a few percent for the more abundant species (such as O, Ne, Mg, and Si) but somewhat higher for the rare species (such as Ar or Ca).

4.4. Sensitivity of the Model to Systematic Uncertainties

Systematic errors may bias the results of the fitting procedure. One source of systematic uncertainty is in the energy response of the TRACER detector. As described by Ave et al. (2008), the energy measurement of TRACER utilizes the relativistic rise in specific ionization in gas (dE/dx), and the detection of transition radiation. The relativistic rise is a weak effect, predicting an increase in signal by 40% ± 2% over the energy range 10–400 GeV amu^{-1}. The uncertainty in this rise is the dominant source of error in the energy measurement. Therefore, the data analysis of TRACER has been repeated assuming relativistic rises of 38% and of 42%. An identical fitting procedure has been performed on the resulting energy spectra as before (where a 40% rise was assumed), and contour maps in (α, Λ_0) have been generated for both cases. As shown in Figure 6, the contour maps exhibit significant overlap. This illustrates the robustness of the model.

Table 1
Relative Source Abundances of Cosmic Ray Nuclei from TRACER (10–10^3 GeV amu^{-1}), Compared with the Universal Elemental Abundances and Normalized to Silicon ($n_{Si} \equiv 100.0$)[a]

Element	*TRACER*	*Universal*	TRACER/Universal
O	532.0 ± 5.0	2089.3 ± 311.0	0.26 ± 0.05
Ne	83.0 ± 1.0	338.8 ± 43.7	0.25 ± 0.04
Mg	124.0 ± 1.0	107.2 ± 11.6	1.16 ± 0.14
Si	100.0 ± 1.0	100.0 ± 10.8	1.00 ± 0.12
S	20.0 ± 1.0	60.2 ± 13.5	0.33 ± 0.10
Ar	5.1 ± 0.4	9.3 ± 2.1	0.55 ± 0.16
Ca	7.1 ± 0.4	6.5 ± 0.3	1.10 ± 0.08
Fe	98.0 ± 1.0	89.1 ± 7.8	1.10 ± 0.11

Note. [a] The relative source abundances correspond to a source spectrum which is a power law in rigidity.

4.5. Monte Carlo Simulations

Monte Carlo simulations have been performed in order to verify that the fitting procedures in Sections 4.2 and 4.3 accurately reconstruct the source parameters α, Λ_0, and n_i. The procedure for these simulations is as follows: first, cosmic ray spectra at the source with index α and source abundances n_i are assumed. The arriving energy spectra are calculated assuming a residual path length Λ_0. Folding these spectra with the acceptance, exposure factor, and efficiencies of the TRACER instrument, a set of simulated measurements is obtained. The number of counts in each energy interval is then fluctuated assuming Poisson statistics.

An identical fit procedure as described for real data is applied to the simulated data and the reconstructed value of (α, Λ_0) is then recorded. New simulated data sets (~10,000) are then generated with the same α, Λ_0, and n_i, and the fitting procedure is repeated for each set in order to obtain a high-statistics test of the method. The resulting reconstructed values of (α, Λ_0) are stored in a two-dimensional histogram and the most probable reconstructed value for (α, Λ_0) is determined. Contours containing 68% and 99% of the reconstructed values of (α, Λ_0) are determined and shown in Figure 8 for two different sets of initial values α, Λ_0, and n_i.

The distributions in Figure 8 reveal that the initial input parameters are quite well reproduced in the fitting procedure. The close agreement between the Monte Carlo simulation, for an input value of (α, Λ_0) = (2.4, 0.3 g cm^{-2}), and the real data in Figure 6 is quite remarkable. It appears that the procedure works well within the framework of the chosen propagation model and provides a good indication of the true source and propagation characteristics.

5. SOURCE ABUNDANCES

The quantities n_i obtained in the fitting procedure (Section 4.2) represent the relative intensities of the primary cosmic ray nuclei at the acceleration site over a large range of energies, from 10 GeV amu^{-1} to several 10^3 GeV amu^{-1}. For the model with (α, Λ_0) = (2.4, 0.3 g cm^{-2}), source abundances (normalized to silicon) are derived and presented in Table 1 ($n_{Si} \equiv$ 100.0) together with statistical uncertainties. The relative source

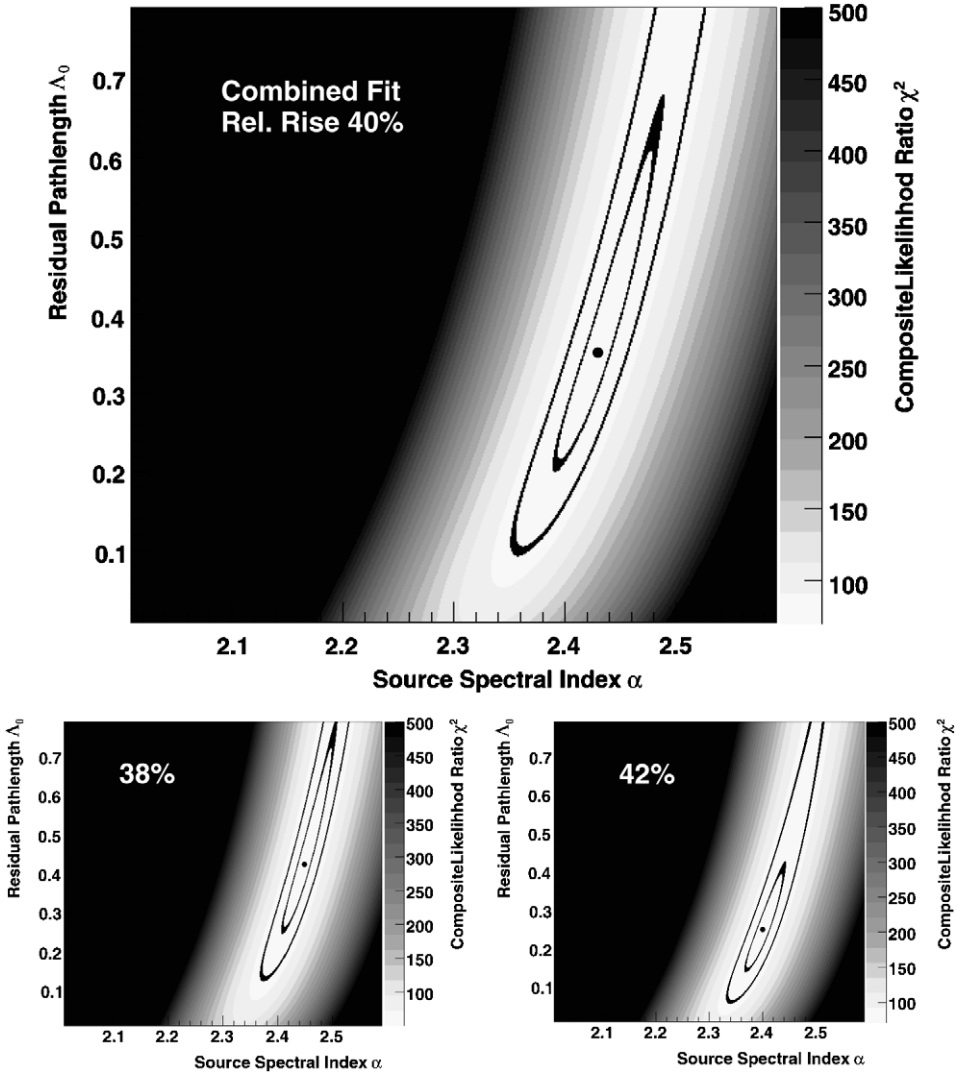

Figure 6. Contour maps of χ^2 values for the combination of eight elements. The 1σ and 3σ contours are indicated. The top plot is for the nominal value of the relativistic rise (40%). The lower plots are for relativistic rises of 38% (lower left) and 42% (lower right). See Section 4.4 for more details.

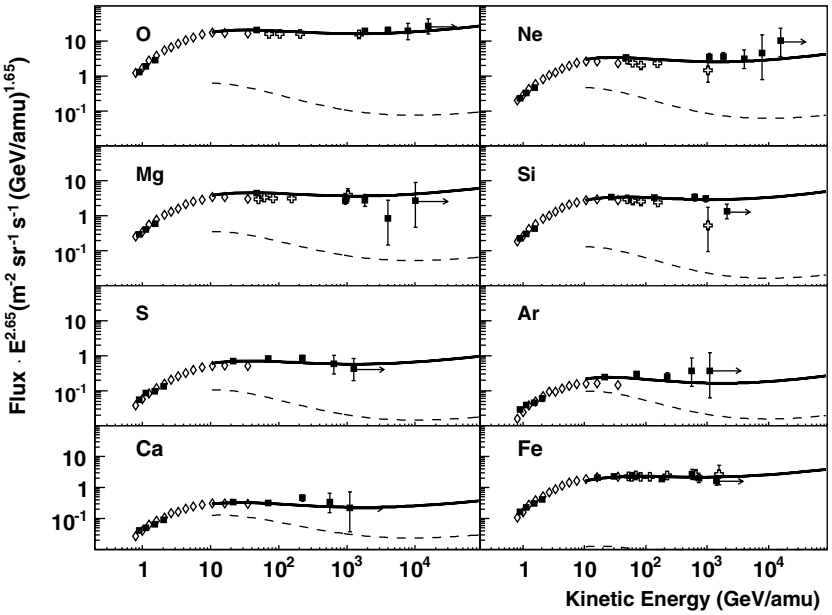

Figure 7. Differential energy spectra, multiplied with $E^{2.65}$, from TRACER (squares), *HEAO-3* (diamonds), and CRN (crosses). The solid curves represent predictions from the propagation model with $(\alpha, \Lambda_0) = (2.4, 0.3\ \mathrm{g\ cm^{-2}})$. The dashed lines show the contribution of secondary particles to the intensities of the individual elements.

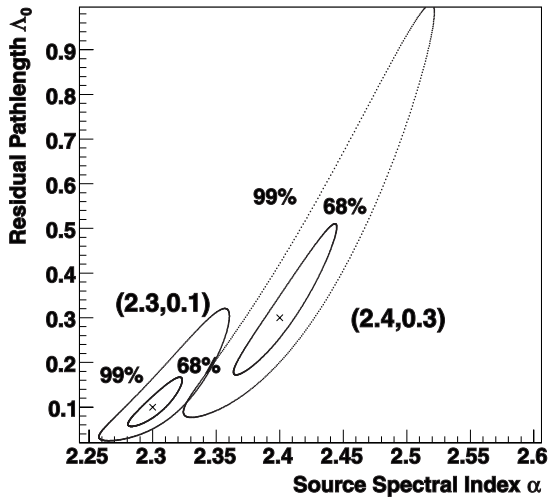

Figure 8. Monte Carlo reconstruction of (α, Λ_0) for simulated data corresponding to input values of $(\alpha, \Lambda_0) = (2.3, 0.1\ \mathrm{g\ cm^{-2}})$ and $(2.4, 0.3\ \mathrm{g\ cm^{-2}})$.

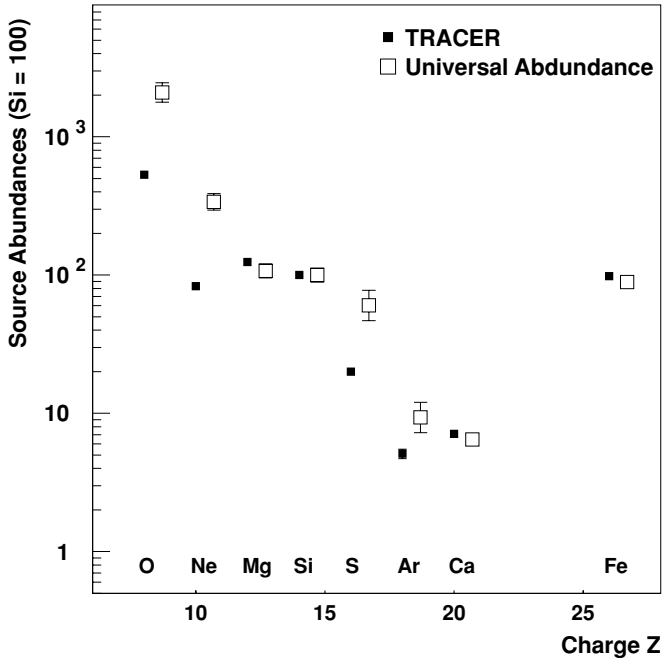

Figure 9. Relative source abundances of cosmic ray nuclei from TRACER (10–10^3 GeV amu^{-1}), compared with the Universal elemental abundances and normalized to silicon. Charge Z is offset for clarity.

abundances have been calculated for a source spectrum which is a power law in rigidity. If the source spectrum is expressed as a power law in energy per amu, all source abundances, relative to silicon, remain the same except for iron as iron is the only observed element with $A/Z > 2$. One then obtains $n_{\mathrm{Fe}} = 82.0$.

Systematic uncertainties in the cross sections result in a 5% error in the source abundances for all elements except argon and calcium where the error is of the order of 20%. The dependence of the source abundance on (α, Λ_0) is relatively minor for values of (α, Λ_0) *along the valley* of the contour plot in Figure 6. The resulting uncertainty is ∼1%. Figures 9 and 10 compare the source abundances from TRACER with the "Universal" abundance scale (Grevesse et al. 1996), and with source abundances derived by the *HEAO-3* and CRN experiments.

Note that the relative source abundances derived in this work for the elements argon and sulfur are higher than that

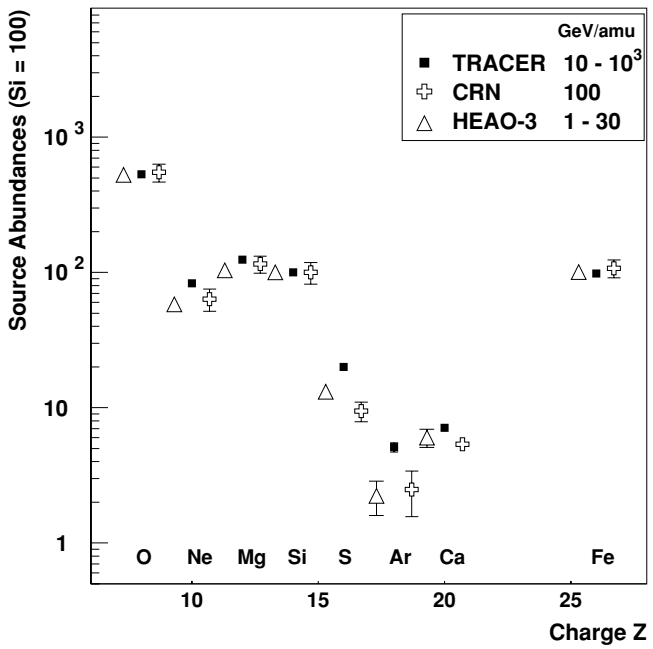

Figure 10. Relative source abundances of cosmic ray nuclei from TRACER (squares), compared with results from *HEAO-3* (triangles) and CRN (crosses). Charge Z is offset for clarity.

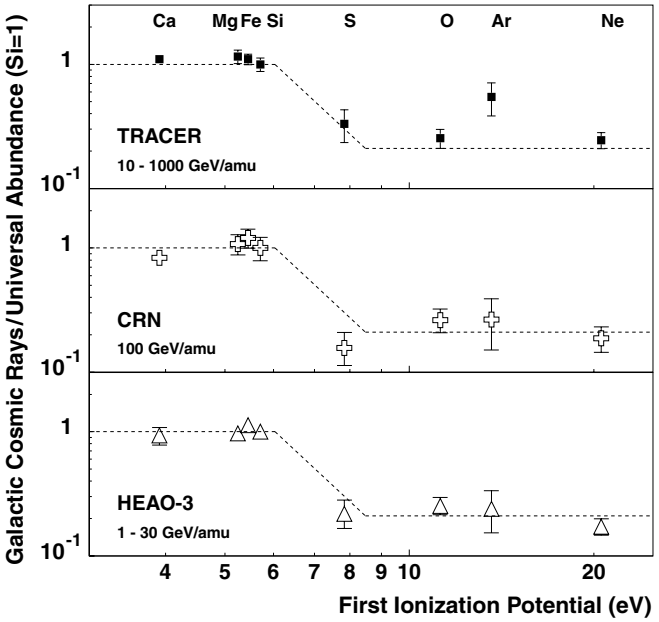

Figure 11. Ratio of the galactic cosmic ray source abundances to the Universal elemental abundances plotted against FIP for TRACER (squares), and compared with results from *HEAO-3* (triangles) and CRN (crosses). Data are normalized to silicon.

previously derived by the CRN and *HEAO-3* experiments. One might suspect that these elements have a systematic bias due to the limited charge resolution of the TRACER experiment. However, we have scrutinized our result by placing various severe selection cuts on the data and we have not found any evidence for contamination from adjacent charges.

It is well known that the cosmic ray source abundances exhibit characteristic differences from the Universal abundance scale of the elements. The differences seem either to be organized by the first ionization potential (FIP) of the elements or by their volatility (e.g., Meyer et al. 1997). These trends

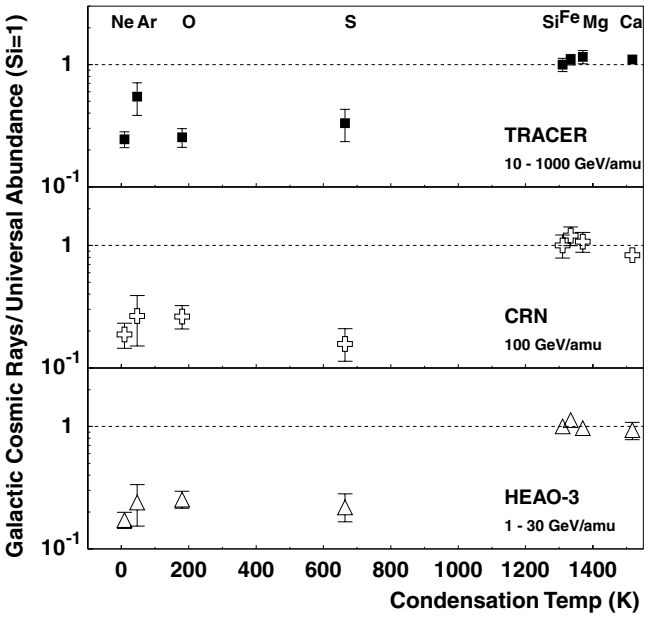

Figure 12. Ratio of the galactic cosmic ray source abundances to the Universal elemental abundances plotted against condensation temperature for TRACER (squares), and compared with results from *HEAO-3* (triangles) and CRN (crosses). Data are normalized to silicon.

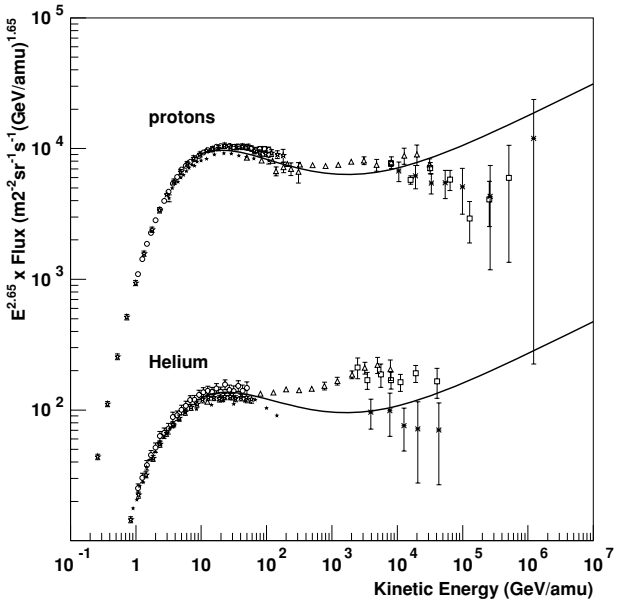

Figure 13. Comparison of the model described in this work with measured energy spectra for protons and helium (see the text for references). The predicted spectra for $(\alpha, \Lambda_0) = (2.4, 0.3\ \mathrm{g\ cm^{-2}})$ are indicated by the solid curves.

are also reflected in the results from TRACER, as shown in Figures 11 and 12.

6. DISCUSSION AND CONCLUSION

We have described a model for the source energy spectra and galactic propagation of cosmic ray nuclei that describes quite well the high-energy measurements made with the TRACER instrument. The model uses physically plausible assumptions: common power-law energy spectra for all components at the sources, and a nonvanishing residual path length for propagation through the galaxy. The strength of the model lies in the fact that it uses a minimum number of free parameters, and that it achieves a self-consistent description of the individual energy spectra of all the heavier primary cosmic ray elements, from $Z = 8$ to $Z = 26$.

The fitting procedure described in this study determines two parameters, the power-law index α for the source energy spectrum, and the residual path length Λ_0. While $(\alpha, \Lambda_0) = (2.4, 0.3\ \mathrm{g\ cm^{-2}})$ are chosen, it is emphasized that this choice is not unique. As Figure 6 indicates, over a certain range lower or higher values of both quantities seem to be possible, provided that these values lie along the valley in the likelihood contour plot. It appears that values from $(\alpha, \Lambda_0) = (2.3, 0.1\ \mathrm{g\ cm^{-2}})$ to $(2.45, 0.6\ \mathrm{g\ cm^{-2}})$ are possible solutions.

To arrive at a unique solution, a number of additional constraints must be considered.

1. *Energy spectra of protons and helium*: the abundant cosmic ray components H and He are not measured with TRACER. Nevertheless, if these nuclei are generated in the same sources and have the same propagation history as the heavier cosmic rays, the shape of their energy spectra can be predicted with the model described here and can be compared with reported measurements (Alcaraz et al. 2000; Asakimori et al. 1998; Boezio et al. 2003; Derbina et al. 2005; Panov et al. 2006; Sanuki et al. 2000). Such a comparison is shown in Figure 13 for $(\alpha, \Lambda_0) = (2.4, 0.3\ \mathrm{g\ cm^{-2}})$. For protons, the model appears to be in rough agreement with the data up to about 10^4 GeV. For helium, the comparison is inconclusive. However, these data extend to higher rigidities than those of the nuclear species covered in the present study and also represent a number of experiments, each with different statistical and systematic uncertainties. Therefore, more scrutiny is required for a detailed analysis, but is beyond the scope of this paper. One might speculate that the high-energy portion of the measured proton spectrum is affected by an intrinsic rigidity cutoff of the SN-shock acceleration mechanism (LaGage & Cesarsky 1983), but this suggestion must remain tentative at present.
2. *Shock acceleration mechanism*: the preferred source power-law index in the model ($\alpha \sim 2.3$–2.4) indicates a fairly soft source energy spectrum. This appears to be difficult to explain in the context of most shock acceleration models which predict harder spectra, with α close to 2.0 for strong shocks (e.g., Bell 1978, and numerous subsequent papers). Figure 6 shows that a relatively small value for the residual path length Λ_0 would imply a harder source spectrum, but not hard enough to easily satisfy the shock-acceleration prediction. One also might ask whether the assumed $E^{-0.6}$ power law represents too strong an energy dependence of the propagation path length. However, a smaller power-law index there would tend to lead to a still softer source spectrum and hence, would aggravate the situation. Clearly, this aspect of our study requires further investigation.
3. *TeV γ-ray observations*: another experimental constraint comes from TeV γ-ray observations of several SNRs in the Galaxy (Aharonian et al. 2004). The energy spectra of the γ rays can be fitted with power-law indices of typically 2.1–2.2. If these γ rays are indeed produced by interactions of hadrons accelerated in the SNR, and if these sources are typical for all cosmic ray accelerators, the source power-law index for cosmic rays could not be larger than about 2.3.
4. *Secondary cosmic ray nuclei*: a direct determination of the cosmic ray propagation path length can be obtained

from measurements of the relative intensities of spallation produced cosmic ray nuclei, e.g., the boron to carbon ratio. If such measurements extended to sufficiently high energies (at least into the TeV per amu region), they would provide the most direct test of the propagation model used in the present study.

To conclude, we believe that to unravel the acceleration and propagation enigma, the next experimental step lies in new composition measurements. These measurements must not only extend the range of energies and improve the available counting statistics, but most importantly, they should include the secondary or mostly secondary nuclei below $Z = 26$ with high precision. Such measurements pose formidable experimental challenges. They require very large exposure factors, excellent charge resolution, and identification of atmospheric background for balloon-borne investigations. We believe that an instrument based on the TRACER concept would be uniquely suited to meet these challenges.

This work was supported by NASA grants NAG5-5305, NN04WC08G, and NNG06WC05G. J.M. acknowledges support from the Illinois Space Grant Consortium.

REFERENCES

Aharonian, F., et al. 2004, Nature, 432, 75
Ahn, H. S., et al. 2008, Astropart. Phys., 30, 3
Alcaraz, J., et al. 2000, Phys. Lett. B, 490, 27
Asakimori, K., et al. 1998, ApJ, 502, 278
Ave, M., Boyle, P. J., Gahbauer, F., Höppner, C., Hörandel, J. R., Ichimura, M., Müller, D., & Romero-Wolf, A. 2008, ApJ, 678, 262
Baker, S., & Cousins, R. D. 1984, Nucl. Instrum. Methods Phys. Res., 221, 437
Bell, A. R. 1978, MNRAS, 182, 147
Boezio, M., et al. 2003, Astropart. Phys., 19, 583
Derbina, V., et al. 2005, ApJ, 628, L41
Engelmann, J., et al. 1990, A&A, 233, 96
Garcia Muñoz, M., Mason, G. M., & Simpson, J. A. 1975, ApJ, 201, L141
Ginzburg, V. L., & Syrovatskii, S. 1964, On the Origin of Cosmic Rays (New York: McMillan)
Grevesse, N., et al. 1996, in ASP Conf. Ser. 99, Cosmic Abundances, ed. S. S. Holt & G. Sonneborn (San Francisco, CA: ASP), 117
Hörandel, J. R., Kalmykov, N. N., & Timokhin, A. V. 2006, J. Phys. Conf. Ser., 47, 132H
Juliusson, E., Meyer, P., & Müller, D. 1972, Phys. Rev. Lett., 29, 445
LaGage, P. O., & Cesarsky, C. J. 1983, A&A, 125, 249
Meyer, J. P., et al. 1997, ApJ, 487, 182
Müller, D., et al. 1991, ApJ, 374, 356
Panov, A., et al. 2007, Bull. Russian Acad. Sci. Phys., 71, 4
Ptuskin, V. S., Völk, H. J., Zirakashvili, V. N., & Breitschwerdt, D. 1997, A&A, 321, 434
Sanuki, T., et al. 2000, ApJ, 545, 1135
Seo, E. S., et al. 2006, Advances in Space Sciences, in press
Smith, L. H., Buffington, A., Smoot, D. F., Alvarez, L. W, & Wahlig, M. A. 1973, ApJ, 180, 987
Swordy, S. P., et al. 1990, ApJ, 349, 625
Villagrasa-Canton, C., et al. 2007, Phys. Rev. C, 75, 044603
Webber, W. R., et al. 1990, Phys. Rev. C, 41, 533
Webber, W. R., et al. 2003, ApJS, 144, 153
Wiedenbeck, M. E., et al. 1998, AAS, 194, 2804H
Yanasak, N. E., et al. 2001, ApJ, 563, 768